Hydrol. Earth Sys. Sci. Discuss., 2, 1449–1502, 2005
www.copernicus.org/EGU/hess/hessd/2/1449/
SRef-ID: 1812-2116/hessd/2005-2-1449
European Geosciences Union

Hydrology and Earth System Sciences Discussions

Papers published in *Hydrology and Earth System Sciences Discussions* are under open-access review for the journal *Hydrology and Earth System Sciences*

Efficient reconstruction of dispersive dielectric profiles using time domain reflectometry (TDR)

P. Leidenberger, B. Oswald, and K. Roth

Institute of Environmental Physics, University of Heidelberg, Heidelberg, Germany

Received: 29 July 2005 – Accepted: 5 August 2005 – Published: 15 August 2005

Correspondence to: B. Oswald (benedikt.oswald@iup.uni-heidelberg.de)

Abstract

We present a numerical model for time domain reflectometry (TDR) signal propagation in dispersive dielectric materials. The numerical probe model is terminated with a parallel circuit, consisting of an ohmic resistor and an ideal capacitance. We derive analytical expressions for the capacitance, the inductance and the conductance of three-wire probes. We couple the time domain model with global optimization in order to reconstruct water content profiles from TDR traces. For efficiently solving the inverse problem we use genetic algorithms combined with a hierarchical parameterization. We investigate the performance of the method by reconstructing synthetically generated profiles. The algorithm is then applied to retrieve dielectric profiles from TDR traces measured in the field. We succeed in reconstructing dielectric and ohmic profiles where conventional methods, based on travel time extraction, fail.

1. Introduction

1.1. Motivation

Time Domain Reflectometry (TDR) has become an indispensable technique for measuring the water content of soils in hydrology, civil engineering, agriculture and related fields over the last years, for a review see Robinson et al. (2003). Early realizations of the method delivered a single water content θ from a TDR trace (Birchak et al., 1974; Topp et al., 1980, 1982a,b; Topp and Davis, 1985; Dasberg and Dalton, 1985). A second phase of TDR development has targeted to deliver spatially resolved water content profiles along the TDR probe (Yanuka et al., 1988; Hook et al., 1992; Dasberg and Hopmans, 1992; Pereira, 1997; Todoroff et al., 1998; Feng et al., 1999; Oswald, 2000; Oswald et al., 2003; Lin, 2003; Heimovaara et al., 2004; Schlaeger, 2005).

Because the dielectric permittivity of soil material typically depends considerably on frequency, particularly if there are clay and loam components (Hoekstra and Delaney, 1974; Sposito and Prost, 1982; Ishida et al., 2000; Huisman et al., 2004; Robinson et al., 2005), in a third phase methods have been studied to recover the average dispersive dielectric parameters from TDR traces (Heimovaara, 1994; Heimovaara et al., 1996; Hilhorst et al., 2001; Lin, 2003). Clearly, the next logical step are methods to extract the full dielectric profile from a TDR trace.

1.2. Objectives

In this paper we study an efficient method for the reconstruction of spatially resolved profiles of water content and electrical conductivity from TDR traces assuming dispersive dielectric properties of the soil material along the probe. In particular, we want to reconstruct field measured TDR traces (Wollschläger and Roth, 2005) which could not be successfully reconstructed with techniques used by Roth et al. (1990).

We use the Debye model to account for dispersive dielectric properties (Debye, 1929). While the three-rod probe is often employed for TDR measurements, there is only scarce material on its transmission line parameters, particularly inductance, capacitance and conductance per unit length. We therefore derive an analytical model for these parameters under the approximation of small conductor diameter D with respect to conductor distance d.

2. Methods

The propagation of TDR signals, voltage $v(x,t)$ and current $i(x,t)$, on probes of two or more conducting rods is described by transmission line theory (e.g. Ramo et al., 1984). Our approach for numerically modeling TDR probes is essentially based on Oswald et al. (2003). A transmission line is described by capacitance C', conductance G', inductance L' and resistance R', all per unit length. These parameters are functions of the probe geometry and the dielectric and ohmic properties of the material between the probe's conductors $C'=C'(d,D,\epsilon)$, $G'=G'(d,D,\sigma)$, $L'=L'(d,D,\mu)$

HESSD

2, 1449–1502, 2005

and $R'=R'(d,D,R_{skin})$ where d is the spacing between the probe rods (for a three wire probe this is the distance between neighboring rods) and D is the diameter of the probe rods.

For piecewise constant transmission line parameters, voltage $v(x,t)$ and current $i(x,t)$ are described by the the following two linear first order, partial differential equations (PDE) (Ramo et al., 1984):

$$\frac{\partial v}{\partial x} = -\left(R' + L'\frac{\partial}{\partial t}\right) i \tag{1}$$

$$\frac{\partial i}{\partial x} = -\left(G' + C'\frac{\partial}{\partial t}\right) v. \tag{2}$$

The piecewise constant dielectric permittivity ϵ and ohmic conductivity σ can be discontinuous, because the water content θ in general is discontinuous across soil boundaries. With a variable water content $\theta(x)$ along the probe the parameters G' and C' vary accordingly; L' is assumed to be constant, because the materials' magnetic permeability equals μ_0; skin resistance R' is neglected in the current study.

For extracting dielectric and ohmic profiles from measured TDR traces we use an iterative, globally optimizing approach based on Oswald et al. (2003), in order to solve the non-linear, inverse, electromagnetic problem. The global optimization method uses genetic algorithms form Levine (1996).

To calculate the TDR signal for a given dielectric profile we numerically solve Eqs. (1) and (2) using a finite difference time domain (FDTD) approach (Taflove, 1998). The spatial discretization of the x coordinate is given by $x=k\Delta x$ and temporal discretization by $t=n\Delta t$ with:

$$\Delta x \leq \frac{\lambda_{\min}}{10} \tag{3}$$

where $\lambda_{\min}$ is the minimum wavelength present in the system, which in non magnetic material, is determined by the maximum frequency $f_{\max}$ and the largest permittivity value ϵ_{max} (Taflove, 1998):

$$\lambda_{min} = \frac{c_0}{f_{max}\sqrt{\epsilon_{r,max}}}. \quad (4)$$

We estimate the maximum relevant frequency from

$$t_{rise} \cdot f_{3dB} = 0.34\,, \quad (5)$$

an expression widely used in electrical engineering. It refers to a Gaussian type time domain waveform with rise time t_{rise}. This is a good model for a TDR input signal. Later on we choose an "explicit" time domain integration. To keep it stable, there is the upper limit for Δt (Taflove, 1998; Kunz and Luebbers, 1993):

$$\Delta t \leq \frac{\Delta x}{c_0} \quad (6)$$

2.1. Numerical solution of transmission line equations

Numerically, there are three spatially different regions, at the beginning of the probe $x=0$, at the end of the probe, $x=\Lambda$, and in-between, $x<0<\Lambda$. At the ends of the probe, the discretized set of PDE is connected to a lumped electrical model, such as voltage sources or resistive-capacitive terminations.

2.1.1. Boundary conditions

The termination of a TDR probe is modeled with a parallel circuit, consisting of an ohmic resistor and an ideal capacitance. The voltage current relationship of this parallel circuit is given by

$$I_T = \frac{V_T}{R_T} + C_T \frac{\partial V_T}{\partial t} \quad (7)$$

where I_T is the current at the end of the TDR probe through the terminal resistor R_T and the terminal capacitance C_T. V_T is the voltage drop at the end of the TDR probe over the parallel circuit of R_T and C_T. To couple this parallel circuit to the distributed transmission line model we use Eq. (1). We truncate the FDTD scheme of the probe through coupling Eqs. (1) and (7) using the definitions:

$$i\,(x=\Lambda,t) = I_T \tag{8}$$

$$v\,(x=\Lambda,t) = V_T\,. \tag{9}$$

We rewrite Eq. (1)

$$\frac{\partial v}{\partial x} = -R'_k i - L'_k \frac{\partial i}{\partial t}\bigg|_{x=\Lambda} \tag{10}$$

$$\Rightarrow \frac{\partial}{\partial x} v\,(x=\Lambda,t) = -R'_K i\,(\Lambda,t) - L'_K \frac{\partial}{\partial t} i\,(\Lambda,t)\,. \tag{11}$$

All current terms in Eq. (11) are replaced by inserting Eq. (7). Note that the currents in the expressions, both constitutive and first-order PDE, are equivalent. Also, the voltages at the end of the probe and across the resistor are equal:

$$\frac{\partial}{\partial x} v\,(\Lambda,t) = -\frac{R'_K}{R_T} v\,(\Lambda,t) - R'_K C_T \frac{\partial}{\partial t} v\,(\Lambda,t) - \frac{L'_K}{R_T}\frac{\partial}{\partial t} v\,(\Lambda,t) - L'_K C_T \frac{\partial^2}{\partial t^2} v\,(\Lambda,t)\,. \tag{12}$$

We select a suitable discretization of Eq. (12): (i) the discretization must result in a fully explicit update scheme; (ii) the scheme must not require values outside the spatial computational domain $x=[0\ldots\Lambda]$. We choose the "backward differencing in space" and "forward differencing in time" scheme using the Taylor series expansion of first-order accuracy. The sum of backward and forward second-order Taylor series expansion in time provides the second order time derivative. With the usual notation we write the discretized version of Eq. (12):

$$\left(\frac{v_K^n - v_{K-1}^n}{\Delta x}\right) = -\frac{R'_K}{R_T} v_K^n - R'_K C_T \left(\frac{v_K^{n+1} - v_K^n}{\Delta t}\right)$$

HESSD

2, 1449–1502, 2005

Efficient and dispersive TDR

P. Leidenberger et al.

$$-\frac{L'_K}{R_T}\left(\frac{v_K^{n+1}-v_K^n}{\Delta t}\right)-L'_K C_T\left(\frac{v_K^{n+1}-2v_K^n+v_K^{n-1}}{\Delta t^2}\right). \tag{13}$$

Finally, by rearranging Eq. (13) we obtain the explicit update procedure, in the time domain, for the voltage at the end of the TDR probe $x=\Lambda$.

$$\begin{aligned} v_K^{n+1} = &\left(\frac{R'_K C_T}{\Delta t}+\frac{L'_K}{R_T\Delta t}+\frac{L'_K C_T}{\Delta t^2}\right)^{-1} \\ &\cdot\left[v_K^n\left(\frac{2L'_K C_T}{\Delta t^2}+\frac{L'_K}{R_T\Delta t}-\frac{R'_K C_T}{\Delta t}-\frac{R'_K}{R_T}-\frac{1}{\Delta x}\right)\right. \\ &\left.-\frac{L'_K C_T}{\Delta t^2}v_K^{n-1}+\frac{1}{\Delta x}v_{K-1}^n\right] \end{aligned} \tag{14}$$

and similarly for the current at $x=\Lambda$ from, using Eq. (7):

$$i_K^{n+1}=\frac{1}{R_T}v_K^{n+1}+C_T\frac{v_K^{n+1}-v_K^n}{\Delta t}. \tag{15}$$

As special cases we mention $C_T=0$, $R_T<\infty$ and $C_T=0$, $R_T\to\infty$. An overview of the equations of all these boundary conditions is given in Table 1. We have implemented them in our TDR code, so almost any given experimental setup can be modeled. The values of C_T and R_T can also be optimized for, if so desired.

To implement the excitation we employ the same approach used by Oswald et al. (2003). We couple a resistive voltage source to the distributed transmission line. The resistive voltage source consists of a series of an ideal ohmic resistor R_S and an ideal voltage source v_S^n. To avoid reflections between the voltage source and the cable connecting the TDR instrument to the probe we adjust R_S to the impedance of the connecting cable. The current flow out of the resistive voltage source is i_S^n. The time derivative of the source voltage is implemented with a discretized version of the given expression for the time domain signal shape.

2.1.2. Transmission line parameters for three-rod TDR Probe

To solve the forward TDR problem the transmission line parameters for the three-rod probe, C', G', L' and R', are essential. Closed-form, analytical expressions for the two-rod probe and the coaxial line are well known (Ramo et al., 1984). This is however not the case for the three-rod probe. We will derive an analytical model for the three-rod TDR probe based on an approximation of the electric and magnetic fields. This approximation, in principle, also applies for the two-rod probe and therefore can be used to assess its quality by comparing it to the exact solution. The comparison is then extrapolated to serve as an indication for the method's reliability to model three-rod probes.

We calculate the electric parameters, C' and G', from the electric potential Φ_{el} and the inductance L' from the magnetic induction $\boldsymbol{B}$ of the three-rod probe. For long rods and a large conductor distance d in comparison to the conductor diameter D, i.e. $\frac{D}{d} \ll 1$, we approximate the electric potential and the magnetic induction. We postulate that the total electrostatic potential of a three-rod probe equals the superposition of the single conductor potentials; the same assumption applies for the magnetic induction. Thus, the neighboring conductors are neglected for the derivation of the potential of a specific conductor. The details of the derivation are given in in Appendix 6. The electrostatic potential, magnetic field, and the geometrical basis of the three-rod probe for calculating these parameters are shown in Fig. 1. The transmission line parameters per unit length for the three rod probe with $\kappa = \frac{d}{D}$ are then obtained as

$$C' = \frac{4\pi\epsilon}{\ln\left(\frac{4\kappa^2-1}{4\kappa-1}\right) + 2\ln(2\kappa-1)} \tag{16}$$

$$G' = \frac{4\pi\sigma}{\ln\left(\frac{4\kappa^2-1}{4\kappa+1}\right) + 2\ln(2\kappa-1)} \tag{17}$$

$$L' = \frac{3\mu_0}{4\pi}\left[\frac{1}{2} + \ln(2\kappa - 1) + \frac{1}{3}\ln\left(\frac{2\kappa+1}{4\kappa-1}\right)\right]. \tag{18}$$

For assessing the quality of the approximate solutions we calculate the electrical parameters for the two-rod probe in the same way:

$$C'_{2,approx.} = \frac{\pi\epsilon\ln(2\kappa)}{\ln(2\kappa-1)} \tag{19}$$

$$G'_{2,approx.} = \frac{\pi\sigma}{\ln(2\kappa-1)} \tag{20}$$

$$L'_{2,approx.} = \frac{\mu_0}{\pi}\left[\frac{1}{2} + \ln(2\kappa-1)\right]. \tag{21}$$

We now calculate the relative error of these approximations using the exact values for the two-rod probe (Ramo et al., 1984):

$$\frac{C'_{2,approx.} - C'_{2,exact}}{C'_{2,exact}} = \frac{\cosh^{-1}(\kappa)}{\ln(2\kappa-1)} - 1 \tag{22}$$

$$\frac{G'_{2,approx.} - G'_{2,exact}}{G'_{2,exact}} = \frac{\cosh^{-1}(\kappa)}{\ln(2\kappa-1)} - 1 \tag{23}$$

$$\frac{L'_{2,approx.} - L'_{2,exact}}{L'_{2,exact}} = \frac{\frac{1}{2} + \ln(2\kappa-1)}{\cosh^{-1}(\kappa)} - 1. \tag{24}$$

The relative error for these three equations is plotted in Fig. 2. The error of the approximation for the capacitance and the conductance is for a wide range much smaller than 4%. For the inductance the error is largely in the range of 10–15%. Transmission line parameters are inherently integral quantities. They result from the integral evaluation of electric (C', G') and magnetic (L') fields, for details Appendix 6. Because the approximation for the two-rod probe is very accurate over a large parameter range, we extrapolate the error of the approximation for the three-rod probe to be of the same size. The quality of the approximation improves with increasing κ, which more and more correspondents to the situation of an infinitely thin line charge and current filament, respectively.

2.2. Time domain dispersive dielectric modeling

Experience gained from TDR traces measured in the field has shown that it is mandatory to consider dispersive dielectric soil properties. We start with a Debye model using one single relaxation frequency (Debye, 1929; Nyfors and Vainikainen, 1989; Taflove, 1998). The Debye model describes the orientation polarization of polar molecules. Let us think of an electric field, switched on instantaneously. The polar molecules turn slowly and the polarization evolves exponentially, with a time constant τ, to its final state. The relative dielectric permittivity ϵ_r as a function of frequency is then:

$$\epsilon_r(\omega) = \epsilon'_\infty + \frac{\epsilon'_s - \epsilon'_\infty}{1 + j\omega\tau}. \tag{25}$$

Here ϵ'_∞ is the permittivity at infinite frequency, where the orientation polarization of the molecules has no time to develop. The static permittivity ϵ'_s corresponds to a state where the orientation polarization has had sufficient time to develop fully. For solving the transmission line equations in the time domain, we transform Eq. (25) into the time domain.

$$\epsilon_r(t) = \epsilon'_\infty \delta(t) + \frac{\Delta\epsilon'}{\tau} e^{-\frac{t}{\tau}} U(t) \tag{26}$$

with $\Delta\epsilon'_r = \epsilon'_s - \epsilon'_\infty$. We end up with a time-dependent capacitance per unit length $C'(t)$, which is split into a time-dependent and a time-independent part:

$$C'(t) = C'_0 \epsilon_r(t) \tag{27}$$

Equation (27) with Eqs. (2) and (1) are discretized, using central finite differences both in space and in time. We obtain the update procedure for the voltage and current:

$$v_k^{n+1} = -\frac{2\Delta t G'_k}{C'_{0k}\epsilon'_{\infty k}} v_k^n - \frac{2\Delta t \Delta\epsilon'_k}{\epsilon'_{\infty k}\tau_k} v_k^n + v_k^{n-1} - \frac{\Delta t}{C'_{0k}\epsilon'_{\infty k}\Delta x}\left(i_{k+1}^n - i_{k-1}^n\right) + \frac{2\Delta\epsilon'_k \Delta t}{\tau_k^2 \epsilon'_{\infty k}} \psi_k^n \tag{28}$$

$$i_k^{n+1} = -\frac{2R'_k \Delta t}{L'_k} i_k^n + i_k^{n-1} - \frac{\Delta t}{\Delta x L'_k}\left(v_{k+1}^n - v_{k-1}^n\right) \tag{29}$$

with the abbreviation

$$\psi_k^n = e^{-\frac{\Delta t}{\tau_k}} \psi_k^{n-1} + \frac{\Delta t}{2}\left(v_k^n + e^{-\frac{\Delta t}{\tau_k}} v_k^{n-1}\right) . \tag{30}$$

The detailed calculation for this discretization can be found in Appendix 7.

2.3. Hierarchical Optimization

Our profile reconstruction approach is based on Oswald et al. (2003). The non-linear inverse problem is solved iteratively with a transmission line solver to calculate TDR traces, based on a given profile of electric parameters. The forward solver is embedded into a global optimizer based on a genetic algorithm (Levine, 1996; Rahmat-Samii and Michielssen, 1999) which delivers electric parameter profiles, adapted according to their fitness. Fitness is a quantity which is roughly inversely proportional to the trace mismatch :

$$m = \sum_{n=N_{start}}^{N_{stop}} \left| v_{meas}(n\Delta t) - v_{calc}(n\Delta t) \right| , \tag{31}$$

We use the sum of absolute values of the difference between calculated and measured TDR traces in contrast to the sum of squared differences used by Oswald et al. (2003).

The genetic algorithm operates on bit-strings which are mapped to real numbers to produces the electric parameter profiles. Hence the electric parameters are inherently discretized. Using a sufficient number of bits per parameter we provide a fine-grained set of values. The efficiency of profile reconstruction depends on the genetic algorithm's parameters: mutation rate, crossover probability and population size. The corresponding values are listed in Tables 3 and 4.

While Oswald et al. (2003) achieve to solve the problem, there are still issues, namely (i) it is computationally intensive due to a large number of forward problem runs (ii) the resulting electric parameter profiles may exhibit oscillatory behavior even if their average corresponds to the converged state.

To alleviate the computational burden and to achieve smoother parameter profiles we have implemented a hierarchical optimization scheme, Fig. 3. The scheme starts out with a coarse spatial resolution which is increased as convergence decreases. For assessing the degree of convergence we calculate the envelope of the fitness and approximate its slope with with a line, Fig. 4. An envelope point (squares at green line) is retrieved as the maximum fitness value of N consecutive individuals, in our case N=30. A complete envelope consists of M such points. As soon as the next N individuals have been calculated, the oldest envelope point is discarded and the whole envelope section is moved one point ahead with respect to the sequence of evaluated individuals. If the majority of envelope points is below the line (red line), with the slope defined in the job file, the spatial resolution is increased by cutting the intervals of dielectric properties into halves. The new intervals are initialized with the same dielectric properties, as the old intervals had at the same location. The optimization stops if a previously specified spatial resolution is reached and the fitness does not increase.

3. Results

3.1. Validation of parallel RC boundary condition

We show the results of TDR traces calculated for different probe termination conditions with a non-dispersive dielectric permittivity between the probe conductors, for all parameters cf. Table 2. Figure 5 shows the open termination. The first reflection results form the cable-probe-transition, the second from the end of the probe. After these, there are multiple reflections. The TDR probe in Fig. 6 is terminated with the probe impedance. There are no reflections from the end of the probe visible, as expected. Figure 7 demonstrates the effect of ohmic conductivity between the probe conductors with an open at the end of the probe. Figure 8 shows the result of a probe with parallel resistive capacitive termination and ohmic conductivity between the probe conductors. At the second reflection we can see the effect of the resistive capacitive termination: (i) at first it behaves like a short circuit; (ii) if the capacitor is charged, it behaves like a pure resistive termination; (iii) and the edges of the reflections are smoothed.

3.2. Validation of dispersive dielectric TDR model

Figures 9–11 show the results for TDR traces calculated with dispersive media and open probe termination. At Fig. 9 the effect of dispersive media with low relaxation frequency can be seen: the reflection coefficient decreases slowly after a reflection. We note that there is negligible ohmic conductivity between the probe rods. Figure 10 shows the second effect of dispersion: the reflections are not sharp any more, they appear smoothed. In Fig. 11 the impact of a smaller $\Delta\epsilon$ with respect to the values used for Fig. 10, is shown.

3.3. Hierarchical reconstruction of water content profiles

3.3.1. Traces measured in non-dispersive media

In Figs. 13–15 we show hierarchical reconstructions of the dielectric parameters for the same traces used by Oswald et al. (2003). The probe was in a sand tank with water content $\theta_1 = \theta_3 = 0$, θ_2 was varied. The experimental setup is sketched in Fig. 12. Relevant optimization parameters are given in Table 3. The vertical dashed lines in fitness and error history indicate an increase in spatial resolution. The number of spatial intervals are given in red in history and fitness.

For Fig. 13 with water content $\theta_2 = 0$ we see no significant increase in fitness, when increasing the spatial resolution during the optimization. For traces with inhomogeneous water content, Fig. 14: $\theta_2 = 0.05$, Fig. 15: $\theta_2 = 0.10$, we see an increase in fitness, if the spatial resolution is commensurate with the region where the water content varies. The hierarchical reconstruction requires about an order of magnitude less iterations for the same traces as the reconstruction with full spatial resolution right from the optimization's start. Additionally, the hierarchical approach leads to considerably smoother profiles when compared to Oswald et al. (2003).

3.3.2. Traces measured under field conditions

In Figs. 16–19 we show hierarchical reconstructions of TDR traces measured under field condition at the Grenzhof (Heidelberg, Germany) test site (Wollschläger and Roth, 2005). The traces were recorded with a "Campbell TDR 100" using a Campbell probe "CS610". Essential TDR properties and the parameters used in the optimization to produce Figs. 16–19 are shown in Table 4. The steps in all these measured traces result of finite time resolution in recording. The first reflection in all traces is a result of the TDR probe head. The head is simulated with a transmission line section. Generally, we can fit the transmission line parameters for this part with our simulation. Because the parameters are constant for every single probe, we fit them manually and fix the respective parameters in the job file, because it would unnecessarily slow down the optimization if it was fitted for every trace from scratch once again. We particularly note Fig. 16. More conventional techniques (e.g. Roth et al., 1990) experience severe problems, may even fail, to evaluate this trace, because there is no sharp reflection from the end of probe.

4. Discussion

We have derived analytical expressions for the transmission line parameters of a three rod probe, based on an approximate model; such expressions, to our knowledge, have not been presented in the area of the TDR literature yet.

We have validated the numerical model by calculating synthetic traces, using both dispersive and non-dispersive dielectric properties. We mention that dispersive dielectrics place additional restrictions onto the time-step of the explicit integration scheme to keep it stable.

We have used a hierarchical approach to reconstruct electric parameter profiles from TDR traces measured in the laboratory with minimal electrical losses. The hierarchical approach reduced the number of forward solutions required and leads to considerably smoother profiles.

We consider hierarchical optimization to be a definite advance and speculate that this will hopefully support the deployment of TDR profile reconstruction in field applications.

Numerical experimentation for reconstructing TDR traces measured in the field has definitely shown that dispersive dielectric properties must be included in the numerical model. Only when using dispersive dielectrics can such TDR traces be recovered numerically; using frequency-independent permittivity alone can not account for the the shape of the traces.

If the frequency range of the TDR instrument is well below the relaxation frequency, dispersion becomes less important. On the other hand, if the TDR's frequency content and the relaxation frequency have a significant overlap, then dispersion will be quite pronounced. The "Campbell TDR 100" has $f_{3dB} \approx 740$ MHz. The relaxation frequencies extracted by the optimization are within this range and therefore dispersion is relevant (Robinson et al., 2003, 2005).

We note that in all cases we used a relatively small mutation probability, 0.01, and a significantly higher cross-over probability, 0.6. Increasing the mutation probability results in a more diverse population but does not seem to accelerate the convergence behavior. On the other hand, using a relatively high cross-over probability ensures efficient reconstruction. The error and fitness histories represent the search in a wide parameter range. For some individuals we obtain a high error and respectively a low fitness. The low fitness of some individuals give the black filled area in fitness history. Note that the error and fitness history are line plots. The high errors are cut of in the plots so that the relevant sector is visible. Additionally, the error's running average is plotted in the diagrams with a blue line.

Furthermore, a more realistic numerical boundary condition using a parallel resistive-capacitive impedance is essential. Using all these model components we succeed in reconstructing field measured TDR traces over a wide spectrum of dielectric permittivity and conductivity. We note that dielectric loss caused by the dispersive Debye model is fundamentally different from electric loss. We finally mention that our profile reconstruction does not require any a priori information whatsoever in order to succeed.

5. Conclusions

A robust, accurate and efficient method has been presented for reconstructing dielectric and ohmic conductivity profiles along TDR traces, for both laboratory and field traces. Different boundary conditions have been implemented for modeling a wide variety of probe terminations encountered in experimental setups. Dispersive dielectric properties are reconstructed and may be of interest for extracting even more information from TDR traces, such as a distinction between bound and free water, so characteristical for clay and loam soils (Ishida et al., 2000).

Now, that TDR technology using conventional, transverse-electric-magnetic (TEM) probes has reached considerable maturity we speculate that it could be worthwhile to address more advanced concepts, such as the single-rod probe using a transverse-magnetic mode of propagation, (Oswald et al., 2004; Nussberger et al., 2005). Such probe types may pose modeling challenges but they also hold the promise of avoiding problems of probes with multiple conducting rods.

The code developed in this work will be available in due course.

6. Appendix: Three-rod probe transmission line parameters

The electric potential of a line charge, with diameter D, in z-direction, cf. Fig. 1, outside the conductor is given by

$$\Phi_{el}(x,y) = \Phi_0 - \frac{Q}{l}\frac{1}{2\pi\epsilon}\ln\left(\sqrt{x^2+y^2}\right) \tag{32}$$

with potential Φ_0 at infinity and line charge density $\frac{Q}{l}$. By convention, the potential at infinity is set to zero. We consider three parallel, infinitely long line charges, Fig. 1. The total potential, outside the conductors, is the superposition of of the single rod potential, Eq. (32):

$$\Phi_{el} = \frac{Q}{l}\frac{1}{2\pi\epsilon}\left\{\frac{1}{2}\ln\left[\left((x-d)^2+y^2\right)\left((x+d)^2+y^2\right)\right] - \ln\left[x^2+y^2\right]\right\}. \tag{33}$$

The capacitance per unit length between conductor 0 and 1 is

$$C'_{01} = \frac{\frac{Q}{l}}{V} \tag{34}$$

with the potential difference V between the two nearest points of conductor 0 and 1:($x{=}D, y{=}0$) and $\left(x{=}d{-}\frac{D}{2}, y{=}0\right)$.

$$V = \Phi_{el}\left(x=\frac{D}{2}, y=0\right) - \Phi_{el}\left(x=d-\frac{D}{2}, y=0\right)$$

$$= \frac{Q}{l} \frac{1}{2\pi\epsilon} \left[\ln\left(\frac{4d^2 - D^2}{4dD - D^2} \right) + \ln\left(\frac{2d - D}{D} \right) \right]. \quad (35)$$

Due to the symmetry of the conductor arrangement the capacitance of a three-rod probe is twice the capacitance, resulting from Eq. (35). Therefore, the capacitance per unit length is

$$C' = \frac{4\pi\epsilon}{\ln\left(\frac{4d^2-D^2}{4dD-D^2}\right) + 2\ln\left(\frac{2d-D}{D}\right)}. \quad (36)$$

The conductance per unit length G' of the medium between the rods is calculated from the electric potential. We use Ohm's law

$$\boldsymbol{j} = \sigma \boldsymbol{E} \quad (37)$$

with current density $\boldsymbol{j}$, ohmic conductivity σ and the electric field $\boldsymbol{E}=-\nabla\Phi_{el}$. The current between conductor 0 and 1 per length l is the integral of $\boldsymbol{j} \cdot F_1$ with $F_1 \perp x$-axis:

$$I = \int_0^l \int_{-\infty}^{+\infty} j_x \, dy \, dz$$

$$= \sigma l \int_{-\infty}^{+\infty} E_x \, dy. \quad (38)$$

Using the electric potential, Eq. (33), and evaluating the integral we obtain

$$I = \frac{\sigma}{\epsilon} Q. \quad (39)$$

With the potential difference, Eq. (35), we compute the conductivity per unit length between conductor 0 and 1:

$$G'_{01} = \frac{I'}{U}. \quad (40)$$

Again, due to the symmetry of the conductor arrangement, Fig. 1, the conductivity per unit length of the three-rod TDR probe is twice G'_{01}:

$$G' = \frac{4\pi\sigma}{\ln\left(\frac{4d^2-D^2}{4dD+D^2}\right) + 2\ln\left(\frac{2d-D}{D}\right)}. \tag{41}$$

The magnetic field of a wire infinitely extended in z-direction with radius $\frac{D}{2}$, conducting current I, using the definition $r=\sqrt{x^2+y^2}$ is

$$r \le \frac{D}{2}: \qquad \boldsymbol{B}(r) = \frac{2\mu_0 I}{\pi D^2} r \tag{42}$$

$$r > \frac{D}{2}: \qquad \boldsymbol{B}(r) = \frac{\mu_0 I}{2\pi r}. \tag{43}$$

The magnetic induction outside a wire for the three-rod probe is given as a superposition of Eq. (43)

$$\boldsymbol{B}(x,y) = \frac{\mu_0 I}{2\pi}\left(\frac{2}{\sqrt{x^2+y^2}} - \frac{1}{\sqrt{(x-d)^2+y^2}} - \frac{1}{\sqrt{(x+d)^2+y^2}}\right) \tag{44}$$

where we have implicitly assumed that we only need the field in a plane parallel to the line connecting the centers of the three conductors, hereby ensuring that the directions of the three magnetic induction components are all parallel. With Eqs. (44) and (42) the magnetic flux Φ_m through the area $F_2 \perp y$-axes with $F_2 = d \cdot l$ at $y=0$ is

$$\begin{aligned}\Phi_m &= l\left[\int_0^{\frac{D}{2}} B_x(x)\,dx + \int_{\frac{D}{2}}^{d-\frac{D}{2}} B_x(x)\,dx + \int_{d-\frac{D}{2}}^{d} B_x(x)\,dx\right] \\ &= \frac{\mu_0 I l}{2\pi}\left[\frac{3}{2} + 3\ln\left(\frac{2d-D}{D}\right) + \ln\left(\frac{2d+D}{4d-D}\right)\right].\end{aligned} \tag{45}$$

The self inductance per unit length between conductor 0 and 1 is

$$L' = \frac{\frac{\Phi_m}{l}}{I}. \tag{46}$$

Due to the symmetry of the arrangement the inductance of the three rod probe is one half the inductance that follows from the magnetic flux Eq. (46). So the inductance per unit length is

$$L' = \frac{3\mu_0}{4\pi}\left[\frac{1}{2} + \ln\left(\frac{2d-D}{D}\right) + \frac{1}{3}\ln\left(\frac{2d+D}{4d-D}\right)\right]. \tag{47}$$

7. Appendix: Discretization of dispersive dielectric medium

To obtain the update procedure for the voltage we insert Eq. (27) into Eq. (2):

$$\begin{aligned}
\frac{\partial i}{\partial x} &= -\left(G' + C'(t)\otimes\frac{\partial}{\partial t}\right)v \\
&= -G'v - C'_0\left[\left(\epsilon'_\infty\delta(t) + \frac{\Delta\epsilon'}{\tau}e^{-\frac{t}{\tau}}U(t)\right)\otimes\frac{\partial v}{\partial t}\right] \\
&= -G'v - C'_0\epsilon'_\infty\int_{-\infty}^{+\infty}\frac{\partial v(t')}{\partial t'}\delta(t-t')\,dt' \\
&\quad -C'_0\frac{\Delta\epsilon'}{\tau}\int_{-\infty}^{+\infty}e^{-\frac{t-t'}{\tau}}U(t-t')\frac{\partial v(t')}{\partial t'}dt'.
\end{aligned} \tag{48}$$

The second term of Eq. (48) is

$$C'_0\epsilon'_\infty\int_{-\infty}^{+\infty}\frac{\partial v(t')}{\partial t'}\delta(t-t')\,dt' = C'_0\epsilon'_\infty\frac{\partial v(t)}{\partial t}. \tag{49}$$

The integral of the third term leads, using partial integration, to

$$\begin{aligned}
\int_{-\infty}^{+\infty} e^{-\frac{t-t'}{\tau}} U\left(t-t'\right) \frac{\partial v\left(t'\right)}{\partial t'} dt' &= \int_{-\infty}^{t} e^{-\frac{t-t'}{\tau}} \frac{\partial v\left(t'\right)}{\partial t'} dt' \\
&= \left[e^{-\frac{t-t'}{\tau}} v\left(t'\right)\right]_{t'=-\infty}^{t'=t} - \int_{-\infty}^{t} \frac{1}{\tau} e^{-\frac{t-t'}{\tau}} v\left(t'\right) dt' \\
&= v\left(t\right) - \frac{1}{\tau} \int_{-\infty}^{t} e^{-\frac{t-t'}{\tau}} v\left(t'\right) dt' . \qquad (50)
\end{aligned}$$

We agree on the following abbreviation:

$$\psi\left(t\right) := \int_{-\infty}^{t} e^{-\frac{t-t'}{\tau}} v\left(t'\right) dt' . \qquad (51)$$

We finally obtain the transmission line Eq. (2) for a Debye medium

$$\frac{\partial i\left(t\right)}{\partial x} = -G' v\left(t\right) - C_0' \epsilon_\infty' \frac{\partial v\left(t\right)}{\partial t} - C_0' \frac{\Delta\epsilon'}{\tau} v\left(t\right) + C_0' \frac{\Delta\epsilon'}{\tau^2} \psi\left(t\right) . \qquad (52)$$

The discretized version of ψ is

$$\begin{aligned}
\psi_k^n &= \psi\left(t\right)\big|_{x_k, t_n} \qquad (53) \\
&= \int_{-\infty}^{n\Delta t} e^{-\frac{n\Delta t - t'}{\tau_k}} v_k\left(t'\right) dt' \qquad (54) \\
&= \int_{-\infty}^{n\Delta t} e^{-\frac{n\Delta t}{\tau_k}} e^{\frac{t'}{\tau_k}} v_k\left(t'\right) dt' \qquad (55)
\end{aligned}$$

$$= e^{-\frac{n\Delta t}{\tau_k}} \left(\int_{-\infty}^{(n-1)\Delta t} e^{\frac{t'}{\tau_k}} v_k(t')\,dt' + \int_{(n-1)\Delta t}^{n\Delta t} e^{\frac{t'}{\tau_k}} v_k(t')\,dt' \right) \tag{56}$$

$$= e^{-\frac{\Delta t}{\tau_k}} e^{-\frac{(n-1)\Delta t}{\tau_k}} \left(\int_{-\infty}^{(n-1)\Delta t} e^{\frac{t'}{\tau_k}} v_k(t')\,dt' + \int_{(n-1)\Delta t}^{n\Delta t} e^{\frac{t'}{\tau_k}} v_k(t')\,dt' \right). \tag{57}$$

With these expansions we write the first integral as a function of ψ_k^{n-1} and the second integral is evaluated using the trapezoidal rule.

$$\psi_k^n = e^{-\frac{\Delta t}{\tau_k}} \psi_k^{n-1} + \frac{1}{2} e^{-\frac{\Delta t}{\tau_k}} e^{-\frac{(n-1)\Delta t}{\tau_k}} \Delta t \left(e^{\frac{n\Delta t}{\tau_k}} v_k^n + e^{\frac{(n-1)\Delta t}{\tau_k}} v_k^{n-1} \right) \tag{58}$$

$$= e^{-\frac{\Delta t}{\tau_k}} \psi_k^{n-1} + \frac{\Delta t}{2} \left(v_k^n + e^{-\frac{\Delta t}{\tau_k}} v_k^{n-1} \right) \tag{59}$$

With this rearrangement we can calculate ψ_k^n from ψ_k^{n-1}. There is no need to save the total history of $v(t)$ which results into a considerable memory savings. The derivatives in Eqs. (52) and (1) are discretized, accurate to 2nd order (Taflove, 1998) using central finite differences both in space and in time. We obtain

$$\frac{i_{k+1}^n - i_{k-1}^n}{2\Delta x} = -G_k' v_k^n - C_{0k}' \epsilon_{\infty k}' \frac{v_k^{n+1} - v_k^{n-1}}{2\Delta t} - C_{0k}' \frac{\Delta \epsilon_k'}{\tau_k} v_k^n + C_{0k}' \frac{\Delta \epsilon_k'}{\tau_k^2} \psi_k^n \tag{60}$$

$$\frac{v_{n+1}^n - v_{k-1}^n}{2\Delta x} = -R_k' i_k^n - L_k' \frac{i_k^{n+1} - i_k^{n-1}}{2\Delta t}. \tag{61}$$

By rearranging terms this leads to the update procedure for voltage and current

$$v_k^{n+1} = -\frac{2\Delta t G_k'}{C_{0k}' \epsilon_{\infty k}'} v_k^n - \frac{2\Delta t \Delta \epsilon_k'}{\epsilon_{\infty k}' \tau_k} v_k^n + v_k^{n-1}$$

$$-\frac{\Delta t}{C'_{0k}\epsilon'_{\infty k}\Delta x}\left(i^n_{k+1}-i^n_{k-1}\right)+\frac{2\Delta\epsilon'_k\Delta t}{\tau^2_k\epsilon'_{\infty k}}\psi^n_k \tag{62}$$

$$i^{n+1}_k=-\frac{2R'_k\Delta t}{L'_k}i^n_k+i^{n-1}_k-\frac{\Delta t}{\Delta x L'_k}\left(v^n_{k+1}-v^n_{k-1}\right). \tag{63}$$

8. List of symbols

B	magnetic field, $\frac{\mathrm{Vs}}{\mathrm{m}^2}=\mathrm{T}$.
c_0	speed of light in vacuum, $\frac{\mathrm{m}}{\mathrm{s}}$.
C	capacitance, F.
C_T	value of the capacitor terminating the TDR probe, F.
C'	capacitance per unit length of a transmission line, $\frac{\mathrm{F}}{\mathrm{m}}$.
Δx	spatial resolution in the discretization of the transmission line equations, m.
$\Delta\epsilon'=\left(\epsilon'_s-\epsilon'_\infty\right)$	difference between static permittivity and permittivity at infinite frequency, dimensionless.
Δt	discretization width in the time domain, s.
D	diameter of the conductors of a two- or three-wire transmission line, m.
d	distance between the centers of two nearest conductors of a transmission line, m.
$\epsilon=\epsilon_0\epsilon_r$	absolute complex dielectric permittivity, $\frac{\mathrm{As}}{\mathrm{Vm}}$.
$\epsilon(t)=\epsilon_0\epsilon_r(t)$	absolute dielectric permittivity as function of time, $\frac{\mathrm{As}}{\mathrm{Vm}}$.
ϵ_0	absolute dielectric permittivity of vacuum, $\frac{1}{\mu c^2}$.

ϵ'_∞	real valued relative permittivity at infinite frequency in Debye model, dimensionless.
ϵ_r	complex valued relative dielectric permittivity, dimensionless.
$\epsilon_{r,\max}$	maximum value of relative dielectric permittivity, dimensionless.
$\epsilon_r(\omega)$	complex valued relative dielectric permittivity as a function of angular frequency of electric field, dimensionless.
$\epsilon_r(t)$	relative dielectric permittivity as a function of time, Fourier transformed of $\epsilon_r(\omega)$, dimensionless.
ϵ'_s	real valued relative permittivity at zero frequency in Debye model, dimensionless.
$\boldsymbol{E}$	electric field, $\frac{\mathrm{V}}{\mathrm{m}}$.
f_{3dB}	frequency at which amplitude of the respective function has reduced by 3dB, Hz.
$f_{\max}$	maximum frequency, Hz.
f_{rel}	relaxation frequency in Debye model, Hz.
G	conductance, S.
G'	conductance per unit length of a transmission line, $\frac{\mathrm{S}}{\mathrm{m}}$.
I	current, A.
I_T	current at the end of the transmission line, A.
$i(x,t)$	current on a transmission line as function of position x and time t, A.
$i_k^n \equiv (x_k, t_n)$	current at point $k\Delta x$ at time $n\Delta t$, A.
i_S	TDR source current, A.
j	imaginary unit, $j = \sqrt{-1}$.
$\boldsymbol{j}$	current density, $\frac{\mathrm{A}}{\mathrm{m}^2}$.
j_x, j_y, j_z	components of current density referring to a Cartesian coordination system, $\frac{\mathrm{A}}{\mathrm{m}^2}$.

$\delta(t)$	Dirac delta function.
$\kappa=\frac{d}{D}$	factor of probe geometry, dimensionless.
k	index used for the specification of spatial locations, $k \cdot \Delta x = x_k$, dimensionless.
K	index, denoting the last index in spatial discretization, $K \cdot \Delta x = \Lambda$, dimensionless.
Λ	total length of TDR-probe, m.
λ_{min}	minimum wavelength, m.
L'	inductance per unit length of a transmission line, $\frac{\mathrm{H}}{\mathrm{m}}$.
l	length of a part of TDR probe, m.
$\mu=\mu_0\mu_r$	magnetic permeability of a material, $\frac{\mathrm{Vs}}{\mathrm{Am}}$.
μ_0	magnetic permeability of vacuum, $4\pi 10^{-7}$, $\frac{\mathrm{Vs}}{\mathrm{Am}}$.
$\mu_r=\left(\mu_r' - j\mu_r''\right)$	complex valued relative magnetic permeability, equals 1 for considered soil materials, dimensionless.
μ_r'	real part of the complex valued relative magnetic permeability, dimensionless.
μ_r''	imaginary part of the complex valued relative magnetic permeability, dimensionless.
M	number of fitness envelope points.
m	mismatch between measured and calculated TDR trace, dimensionless.
N	number of consecutive individuals, used for a fitness envelope point.
N_{start}	index denoting start time for mismatch calculating, dimensionless.
N_{stop}	index denoting stop time for mismatch calculating, dimensionless.
n	index used for the specification of time, $x\left(n \cdot \Delta t\right) = x^n$, dimensionless.

HESSD

2, 1449–1502, 2005

Efficient and dispersive TDR

P. Leidenberger et al.

ω	angular frequency of electric field, $\frac{1}{\mathrm{s}}$.
Φ_{el}	electro static potential, V.
ψ_k^n	$= e^{-\frac{\Delta t}{\tau_k}} \psi_k^{n-1} + \frac{\Delta t}{2} \left(v_k^n + e^{-\frac{\Delta t}{\tau_k}} v_k^{n-1} \right)$, abbreviation for calculations in a dispersive dielectric medium.
Q	electric charge, As.
ρ	reflection coefficient, dimensionless.
R'	resistance per unit length of a transmission line, $\frac{\Omega}{\mathrm{m}}$.
R_S	source impedance of resistive voltage source, Ω.
R_{skin}	skin resistance of a conductor, Ω.
R_T	value of the resistor terminating the TDR probe, Ω.
$\sigma(x)$	ohmic conductivity as a function of longitudinal position on the TDR probe, $\frac{\mathrm{S}}{\mathrm{m}}$.
$\tau = \frac{1}{2\pi f_{rel}}$	relaxation time of a dipole in the Debye model, s.
θ	volumetric water content, $\frac{\mathrm{m}^3}{\mathrm{m}^3}$.
$\theta(x)$	volumetric water content as function of longitudinal position on the TDR probe, $\frac{\mathrm{m}^3}{\mathrm{m}^3}$.
t	time, s.
t_{rise}	rise time of an electrical signal, usually the time required for the signal to rise from 10 to 90% of its final value, s.
t_{sec}	time step security for explicit time domain integration, s.
V_T	voltage at the end of the transmission line, V.
$v(x,t)$	voltage on a transmission line as function of position x and time t, V.
$v_k^n \equiv v(x_k, t_n)$	voltage at point $k\Delta x$ at time $n\Delta t$, V.
v_S	TDR source voltage, V.
$U(t)$	Heaviside step function.
x, y, z	spatial coordinate, m.

Acknowledgements. Financial support of this work was provided in part by Deutsche Forschungsgemeinschaft (Project No. 1080-8/2).

References

Birchak, J. R., Gardner, C. G., Hipp, J. E., and Victor, J. M.: High Dielectric Constant Microwave Probes for Sensing Soil Moisture, Proceedings of the IEEE, 62, 93–98, 1974. 1450

Dasberg, S. and Dalton, F. N.: Time Domain Reflectometry Field Measurements of Soil Water Content and Electrical Conductivity, Soil Sci. Soc. Am. J., 49, 293–297, 1985. 1450

Dasberg, S. and Hopmans, J. W.: Time Domain Reflectometry Calibration for Uniformly and Nonuniformly Wetted Sand and Clayed Loam Soils, Soil Sci. Am. J., 56, 1341–1345, 1992. 1450

Debye, P.: Polare Molekeln, Verlag von S. Hirzel, Leipzig, 1929. 1451, 1458

Feng, W., Lin, C. P., Deschamps, R. J., and Drnevich, V. P.: Theoretical model of a multisection time domain reflectometry measurement system, Water Resources Research, 35, 2321–2331, 1999. 1450

Heimovaara, T. J.: Frequency domain analysis of time domain reflectometry waveforms, 1. Measurement of the complex dielectric permittivity of soils, Wat. Resour. Res., 2, 189–200, 1994. 1451

Heimovaara, T. J., de Winter, E. J. G., van Loon, W. K. P., and Esveld, D. C.: Frequency-dependent dielectric permittivity from 0 to 1 GHz: Time domain reflectometry measurements compared with frequency domain network analyzer measurements, Wat. Resour. Res., 32, 3603–3610, 1996. 1451

Heimovaara, T. J., Huisman, J. A., Vrugt, J. A., and Bouten, W.: Obtaining the Spatial Distribution of Water Content along a TDR probe Using the SCEM-UA Bayesian Inverse Modeling Scheme, Vadose Zone Journal, 3, 1128–1145, 2004. 1450

Hilhorst, M. A., Dirksen, C., Kampers, F. W. H., and Feddes, R. A.: Dielectric Relaxation of Bound Water versus Soil Matric Pressure, Soil Science Society of America Journal, 65, 311–314, 2001. 1451

Hoekstra, P. and Delaney, A.: Dielectric Properties of Soils at UHF and Microwave Frequencies, J. Geophys. Res., 79, 1699–1708, 1974. 1450

Hook, W. R., Livingston, N. J., Sun, Z. J., and Hook, P. B.: Remote Diode Shorting Improves

Measurement of Soil Water by Time Domain Reflectometry, Soil Sci. Am. J., 56, 1384–1391, 1992. 1450

Huisman, J. A., Bouten, W., and Vrugt, J. A.: Accuracy of frequency domain analysis scenarios for the determination of complex dielectric permittivity, Wat. Resour. Res., 40, 1–12, 2004. 1451

Ishida, T., Makino, T., and Wang, C.: Dielectric-relaxation spectroscopy of kaolinite, montmorillonite, allophane, and imogolite under moist conditions, Clays and Clay Minerals, 48, 75–84, 2000. 1451, 1464

Kunz, K. S. and Luebbers, R. J.: The Finite Difference Time Domain Method for Electromagnetics, CRC Press, 2000 Corporate Blvd., N. W., Boca Raton, Florida, 1993. 1453

Levine, D.: Users Guide to the PGAPack Parallel Genetic Algorithm Library, Tech. rep., Argonne National Laboratory 95/18, 9700 South Cass Avenue, Argonne Il 60439, 1996. 1452, 1459

Lin, C. P.: Analysis of non-uniform and dispersive time domain reflectometry measurement systems with application to the dielectric spectroscopy of soils, Wat. Resour. Res., 39, 2003. 1450, 1451

Nussberger, M., Benedickter, H. R., Bächtold, W., Flühler, H., and Wunderli, H.: Single-Rod Probes for Time Domain Reflectometry: Sensitivity and Calibration, Vadose Zone Journal, 4, 551–557, doi:10.2136/vzj2004.0093, 2005. 1465

Nyfors, E. and Vainikainen, P.: Industrial Microwave Sensors, ARTECH HOUSE, INC., 685 Canton Street, Norwood, MA 02062, USA, 1989. 1458

Oswald, B.: Full Wave Solution of Inverse Electromagnetic Problems – Applications in Environmental Measurement Techniques, Ph.D. thesis, Swiss Federal Institute of Technology, Zurich, 2000. 1450

Oswald, B., Benedickter, H. R., Bächtold, W., and Flühler, H.: Spatially resolved water content profiles from inverted TDR signals, Wat. Resour. Res., 39, doi:10.1029/2002WR001890, 2003. 1450, 1451, 1452, 1455, 1459, 1460, 1462, 1495

Oswald, B., Benedickter, H. R., Bächtold, W., and Flühler, H.: A single rod probe for time domain reflectometry, Vadose Zone Journal (VZJ), 3, 1152–1159, 2004. 1465

Pereira, D. S.: Développement d'une nouvelle méthode de détermination des profils de teneur en eau dans les sols par inversion d'un signal TDR, Ph.D. thesis, Lab. d'Etude des Transf. en Hydrol. et Environ (LTHE), Univ. Joseph Fourier-Grenoble I, Grenoble, France, 1997. 1450

Rahmat-Samii, Y. and Michielssen, E.: Electromagnetic Optimization by Genetic Algorithms, Wiley Series in Microwave and Optical Engineering, John Wiley & Sons, 1999. 1459

Ramo, S., Whinnery, J. R., and Duzer, T. V.: Fields and Waves in Communication Electronics, John Wiley & Sons, New York, 2 edn., 1984. 1451, 1452, 1456, 1457

Robinson, D. A., Jones, S. B., Wraith, J. M., Or, D., and Friedman, S. P.: A Review of Advances in Dielectric and Electrical Conductivity Measurements in Soils Using Time Domain Reflectrometry, Vadose Zone J., 2, 444–475, 2003. 1450, 1464

Robinson, D. A., Schaap, M. G., Or, D., and Jones, S. B.: On the effective measurement frequency of time domain reflectometry in dispersive and non-conductive dielectric materials, Wat. Resour. Res., 41, 2005. 1451, 1464

Roth, K., Schulin, R., Flühler, H., and Attinger, W.: Calibration of Time Domain Reflectometry for Water Content Measurement Using a Composite Dielectric Approach, Wat. Resour. Res., 26, 2267–2273, 1990. 1451, 1463

Schlaeger, S.: A fast TDR-inversion technique for the reconstruction of spatial soil moisture content, Hydrol. Earth Syst. Sci. Discuss., 2, 971–1009, 2005, SRef-ID: 1812-2116/hessd/2005-2-971. 1450

Sposito, G. and Prost, R.: Structure of Water Adsorbed on Smectites, Chemical Reviews, 82, 553–573, 1982. 1451

Taflove, A.: Computational electrodynamics: the finite difference time domain method, Artech House, Norwood, Massachusetts, 1998. 1452, 1453, 1458, 1470

Todoroff, P., Lorion, R., and Lan Sun Luk, J. D.: L'utilisation des algorithmes génétiques pour l'identification de profil hydriques de sol a partir de courbes réflectrométriques, C. R. Acad. Sci. Ser. IIa, Sci. Terre Planetes, 327, 607–610, 1998. 1450

Topp, G. C. and Davis, J. L.: Measurement of Soil Water Content using Time-domain Reflectometry (TDR): A Field Evaluation, Soil Sci. Am. J., 49, 19–24, 1985. 1450

Topp, G. C., Davis, J. L., and Annan, A. P.: Electromagnetic Determination of Soil Water Content: Measurement in Coaxial Transmission Lines, Wat. Resour. Res., 16, 574–582, 1980. 1450

Topp, G. C., Davis, J. L., and Annan, A. P.: Electromagnetic Determination of Soil Water Content Using TDR: I. Applications to Wetting Fronts and Steep Gradients, Soil Sci. Am. J., 46, 672–678, 1982a. 1450

Topp, G. C., Davis, J. L., and Annan, A. P.: Electromagnetic Determination of Soil Water Content Using TDR: II. Evaluation of Installation and Configuration of Parallel Transmission Lines, Soil Sci. Am. J., 46, 678–684, 1982b. 1450

Wollschläger, U. and Roth, K.: Estimation of Temporal Changes of Volumetric Soil Water Content from Ground-Penetrating Radar Reflections, Subsurface Sensing Technologies and Applications, 6, 2005. 1451, 1462

Yanuka, M., Topp, G. C., S., Z., and Zebchuk, W. D.: Multiple Reflection and Attenuation of Time Domain Reflectometry Pulses: Theoretical Considerations for Applications to Soil and Water, Wat. Resour. Res., 24, 939–944, 1988. 1450

Table 1. Summary of boundary conditions.

termination condition	voltage	current
parallel resistive capacitive termination 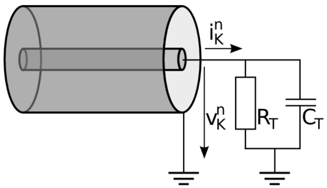 	$v_K^{n+1} = \left(\frac{R'_K C_T}{\Delta t} + \frac{L'_K}{R_T \Delta t} + \frac{L'_K C_T}{\Delta t^2}\right)^{-1} \cdot \left[v_K^n \left(\frac{2L'_K C_T}{\Delta t^2} + \frac{L'_K}{R_T \Delta t} - \frac{R'_K C_T}{\Delta t} - \frac{R'_K}{R_T} - \frac{1}{\Delta x} \right) - \frac{L'_K C_T}{\Delta t^2} v_K^{n-1} + \frac{1}{\Delta x} v_{K-1}^n \right]$	$i_K^{n+1} = \frac{1}{R_T} v_K^{n+1} + C_T \frac{v_K^{n+1} - v_K^n}{\Delta t}$
resistive termination 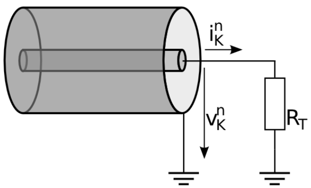 	$v_K^{n+1} = v_K^n \left(1 - \frac{R'_K \Delta t}{L'_K} - \frac{\Delta t R_T}{L'_K \Delta x}\right) + v_{K-1}^n \frac{\Delta t R_T}{L'_K \Delta x}$	$i_k^{n+1} = \frac{1}{R_T} v_K^{n+1}$

HESSD

2, 1449–1502, 2005

Efficient and dispersive TDR

P. Leidenberger et al.

EGU

Table 1. Continued.

termination condition	voltage	current
open termination 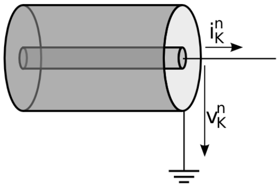	$v_K^{n+1} = v_{K-1}^{n+1}$	$i_K^{n+1} = 0$
resistive voltage source termination 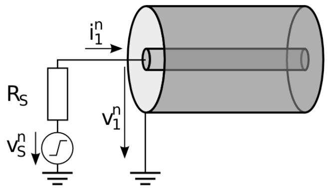	$v_k^{n+1} = v_k^n \left(1 - \frac{\Delta t R_1'}{L_1'} \frac{\Delta t R_S}{L_1' \Delta x}\right) + \frac{\Delta t R_S}{L_1' \Delta x} v_{k+1}^n + \frac{\Delta t R_1'}{L_1'} v_S^n + \Delta t \frac{\partial v_S^n}{\partial t}$	$i_1^{n+1} = \frac{v_S^{n+1}(t) - v_1^{n+1}}{R_S}$

HESSD

2, 1449–1502, 2005

Efficient and dispersive TDR

P. Leidenberger et al.

Table 2. Parameters used for calculation of synthetic TDR traces for validating the termination condition and the dispersive media, for all: ϵ'_∞=10, Δx=$1.2 \cdot 10^{-3}$ m.

Figure number	$\Delta\epsilon'$	f_{rel} (MHz)	σ' ($\frac{\mathrm{S}}{\mathrm{m}}$)	R_T (Ω)	C_T (F)	t_{sec}
5	-	-	$1 \cdot 10^{-30}$	-	-	0.25
6	-	-	$1 \cdot 10^{-30}$	84	-	0.25
7	-	-	$1 \cdot 10^{-2}$	-	-	0.25
8	-	-	$5 \cdot 10^{-3}$	150	$5 \cdot 10^{-12}$	0.25
9	10	10	$1 \cdot 10^{-30}$	-	-	0.25
10	10	100	$1 \cdot 10^{-30}$	-	-	0.11
11	5	100	$1 \cdot 10^{-30}$	-	-	0.25

Table 3. Parameters used for hierarchical TDR trace reconstruction of laboratory traces.

optimization parameter	value
population size	50
crossover probability	0.6
mutation probability	0.01
bits for ϵ_r'	20
bits for conductivity	20
transmission line termination	resistive
termination resistor	214 Ω
TDR rise time t_{rise}	28 ps
spatial discretization	0.0005 m
time step security	0.9
TDR probe type	two rod
probe length	1.0 m
conductor diameter D	1.0 mm
conductor center distance d	30.8 mm

Table 4. Parameters used for hierarchical TDR trace reconstruction of field data.

TDR/optimization parameter	value
population size	50
crossover probability	0.6
mutation probability	0.01
bits for ϵ'_∞	20
bits for $\Delta\epsilon'$	20
bits for f_{rel}	20
bits for conductivity	20
bits for terminal resistor	10
bits for terminal capacitor	10
transmission line termination	parallel resistive capacitive, optimized
TDR rise time t_{rise}	460 ps
measured samples	251
time between samples	107 ps
spatial discretization	0.002 m
time step security	0.25
TDR probe type	three rod
probe length	0.3 m
conductor diameter D	4.8 mm
conductor center distance d	22.5 mm

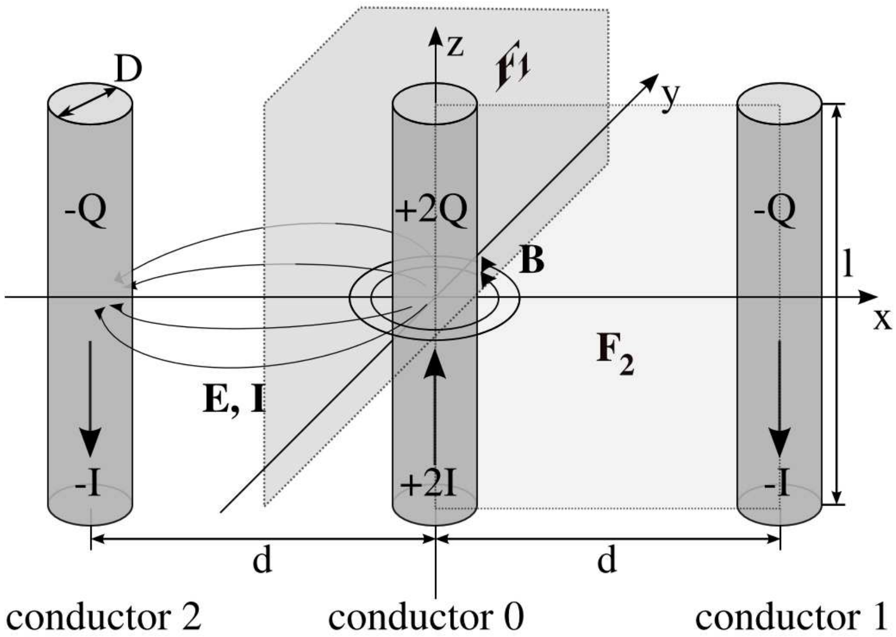

Fig. 1. Three-rod probe configuration and parameters.

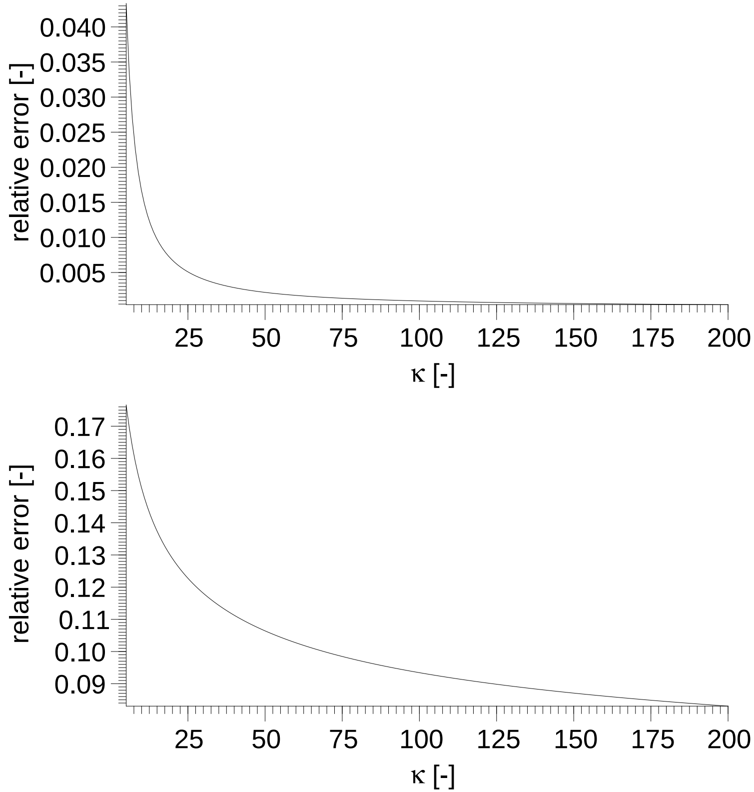

Fig. 2. Relative error of approximated transmission line parameters per unit length to exact parameters for two-rod probe as function of κ. Upper figure: Relative error of capacitance $C'_{2,approx.}$ (conductance $G'_{2,approx.}$) to $C'_{2,exact}$ ($G'_{2,exact}$). Lower figure: Relative error of inductance $L'_{2,approx.}$ to $L'_{2,exact}$.

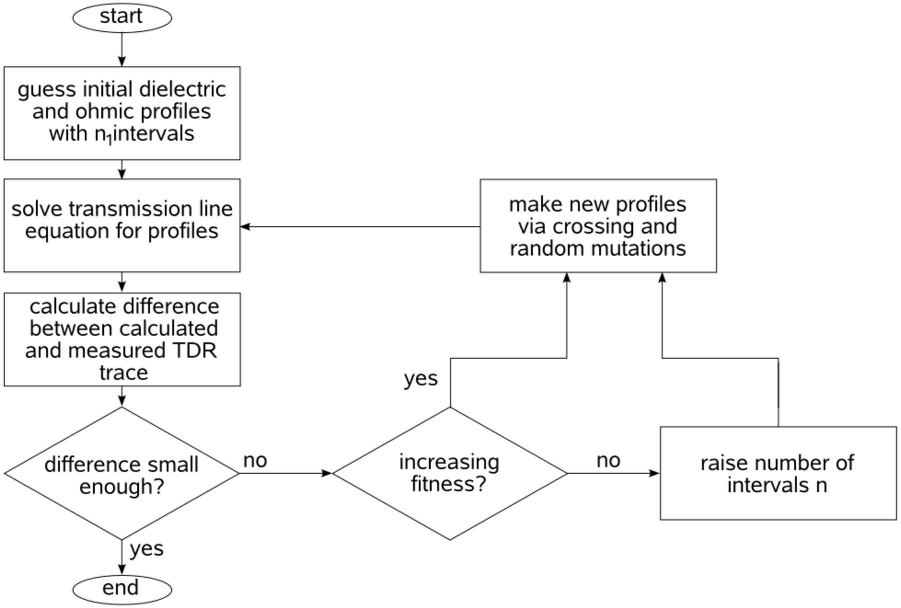

Fig. 3. Flowchart for the hierarchical optimization.

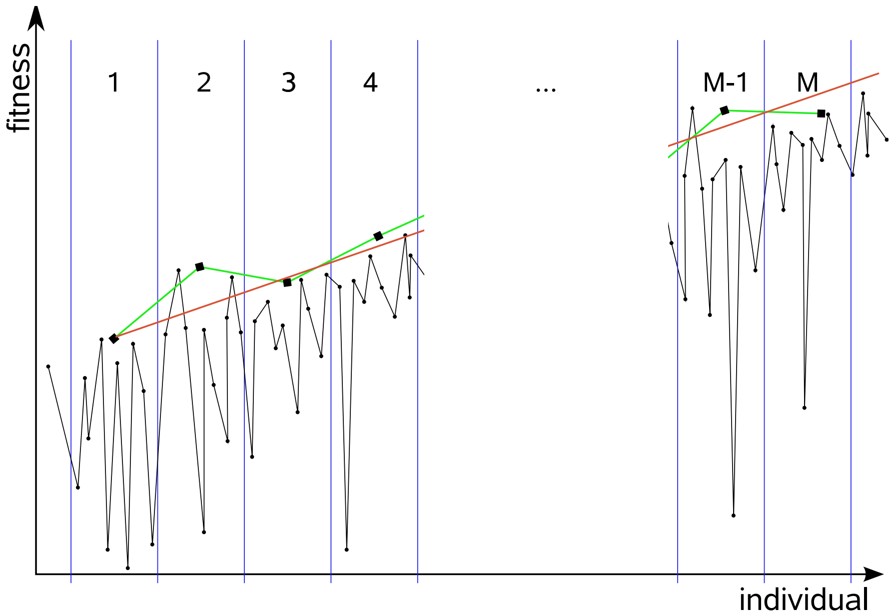

Fig. 4. Determination of the criteria when to increment spatial resolution.

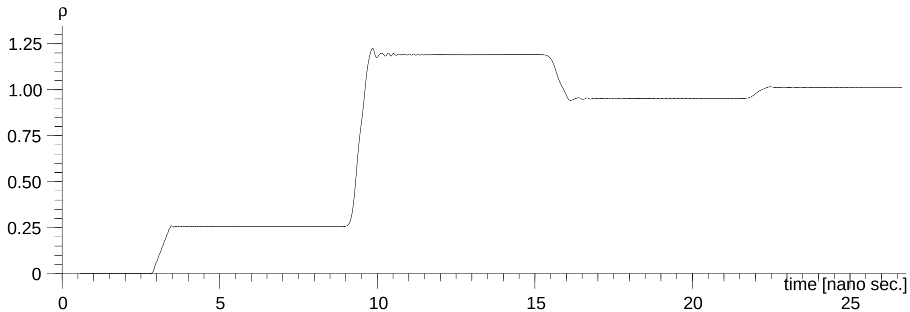

Fig. 5. Calculated TDR trace for two-rod probe with length l=0.3 m, D=4.8 mm, d=22.5 mm, ϵ'_∞=10, σ=10^{-30} S, not dispersive, infinite termination.

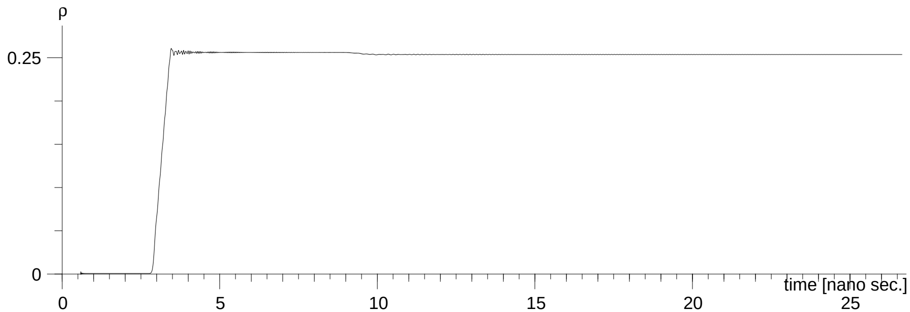

Fig. 6. Calculated TDR trace for two-rod probe with length l = 0.3 m, D = 4.8 mm, d = 22.5 mm, ϵ'_∞ = 10, $\sigma = 10^{-30}$ S, not dispersive, resistive termination, R_T = 84 Ω.

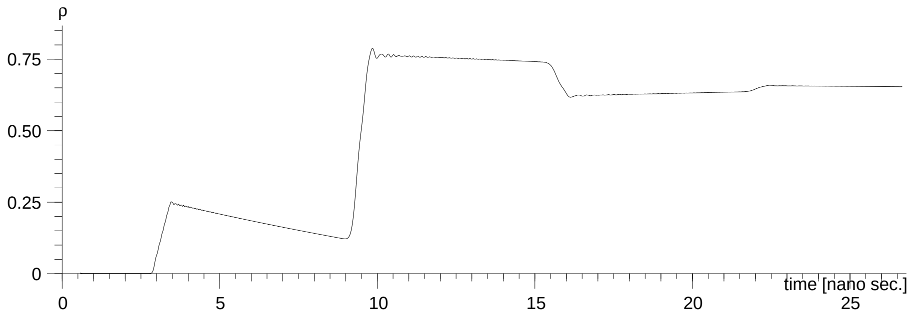

Fig. 7. Calculated TDR trace for two-rod probe with length l = 0.3 m, D = 4.8 mm, d = 22.5 mm, ϵ'_∞ = 10, $\sigma = 1 \cdot 10^{-2}$ S, not dispersive, infinite termination.

HESSD
2, 1449–1502, 2005

Title Page
Abstract
Introduction
Conclusions
References
Tables
Figures
◀I
▶I
◀
▶
Back
Close
Full Screen / Esc
Print Version
Interactive Discussion

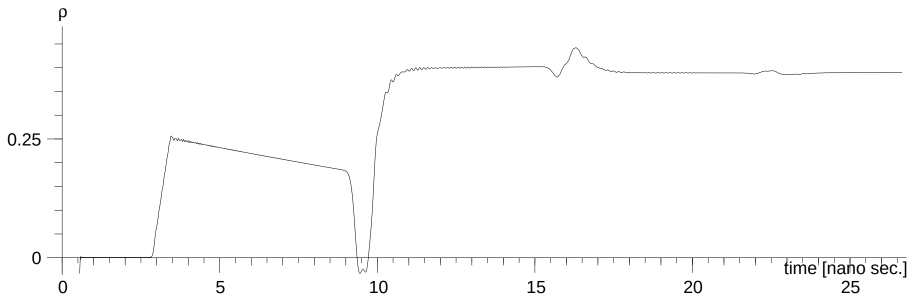

Fig. 8. Calculated TDR trace for two-rod probe with length l = 0.3 m, D = 4.8 mm, d = 22.5 mm, ϵ'_∞ = 10, $\sigma = 5 \cdot 10^{-3}$ S, not dispersive, parallel resistive capacitive termination, R_T = 150 Ω, $C_T = 5.0 \cdot 10^{-12}$ F.

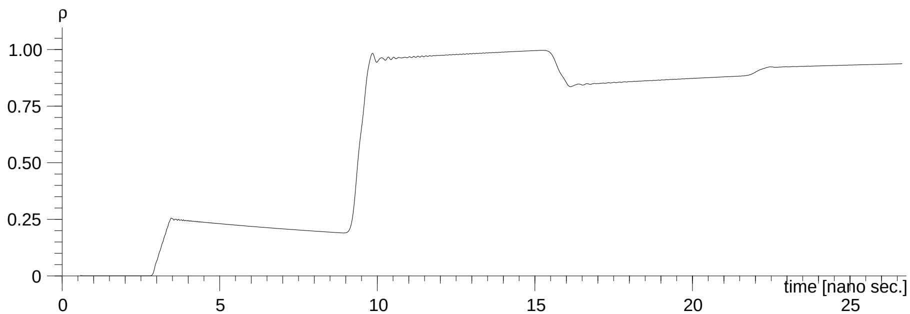

Fig. 9. Calculated TDR trace for two-rod probe with length l = 0.3 m, D = 4.8 mm, d = 22.5 mm, ϵ'_∞ = 10, $\sigma = 1 \cdot 10^{-30}$ S, infinite termination, dispersive media with $\Delta\epsilon'$ = 10, f_{rel} = 10 MHz.

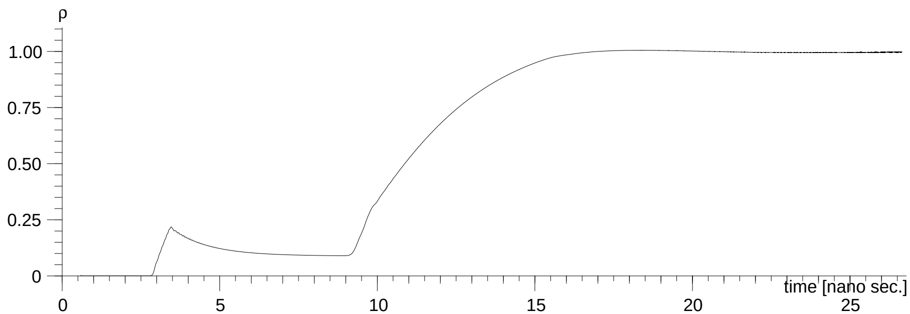

Fig. 10. Calculated TDR trace for two-rod probe with length l = 0.3 m, D = 4.8 mm, d = 22.5 mm, ϵ'_∞ = 10, $\sigma = 1 \cdot 10^{-30}$ S, infinite termination, dispersive media with $\Delta\epsilon'$ = 10, f_{rel} = 100 MHz.

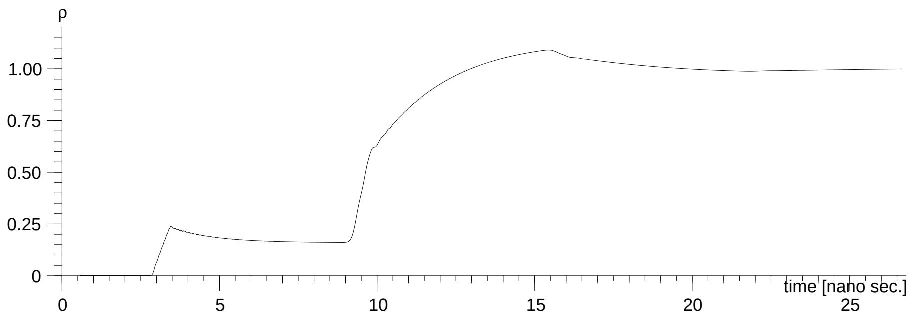

Fig. 11. Calculated TDR trace for two-rod probe with length l = 0.3 m, D = 4.8 mm, d = 22.5 mm, ϵ'_∞ = 10, $\sigma = 1 \cdot 10^{-30}$ S, infinite termination, dispersive media with $\Delta\epsilon'$ = 5, f_{rel} = 100 MHz.

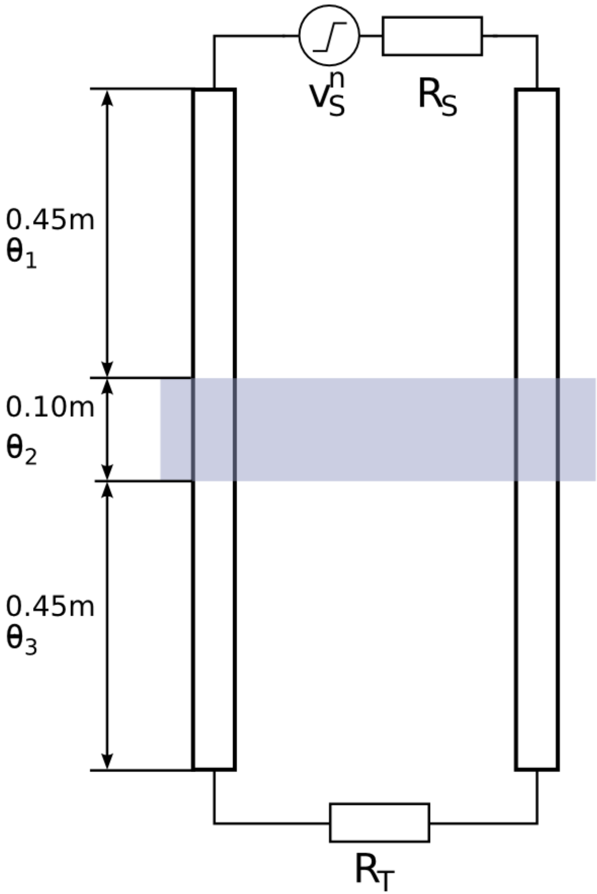

Fig. 12. Experimental setup by Oswald et al. (2003): segmented sand tank with different water contents.

HESSD

2, 1449–1502, 2005

Efficient and dispersive TDR

P. Leidenberger et al.

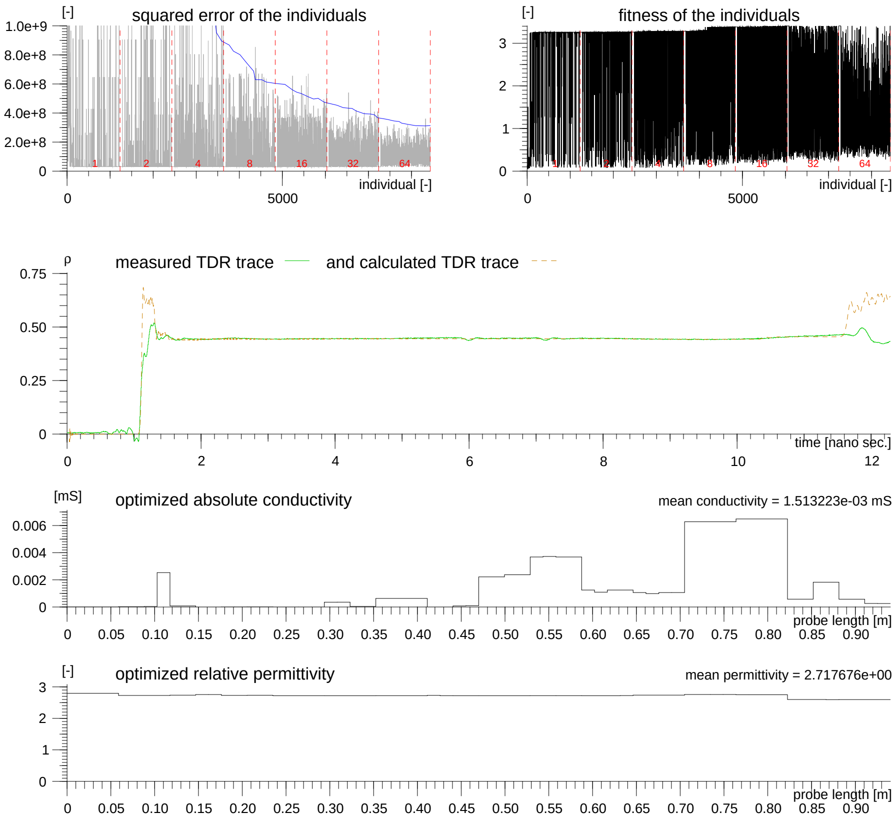

Fig. 13. Reconstruction of synthetic profile, $\theta_2 = 0$. Individual 7547 with error: $2.9 \cdot 10^7$ and fitness: 3.4.

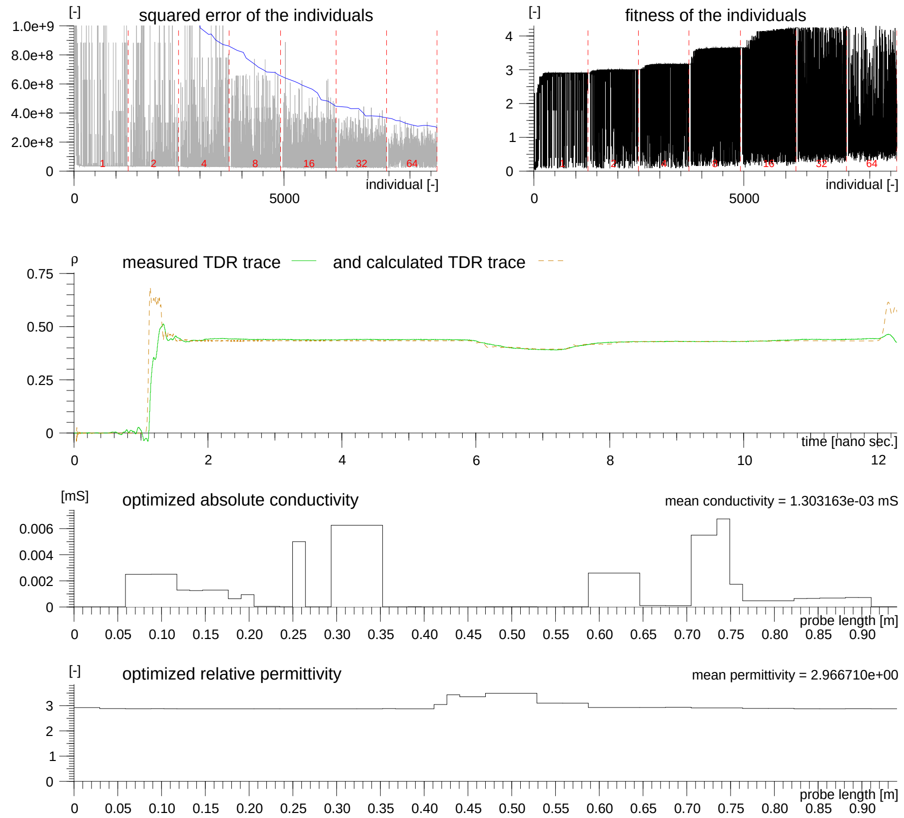

Fig. 14. Reconstruction of synthetic profile, $\theta_2 = 0.05$. Individual 8146 with error: $2.3 \cdot 10^7$ and fitness: 4.3.

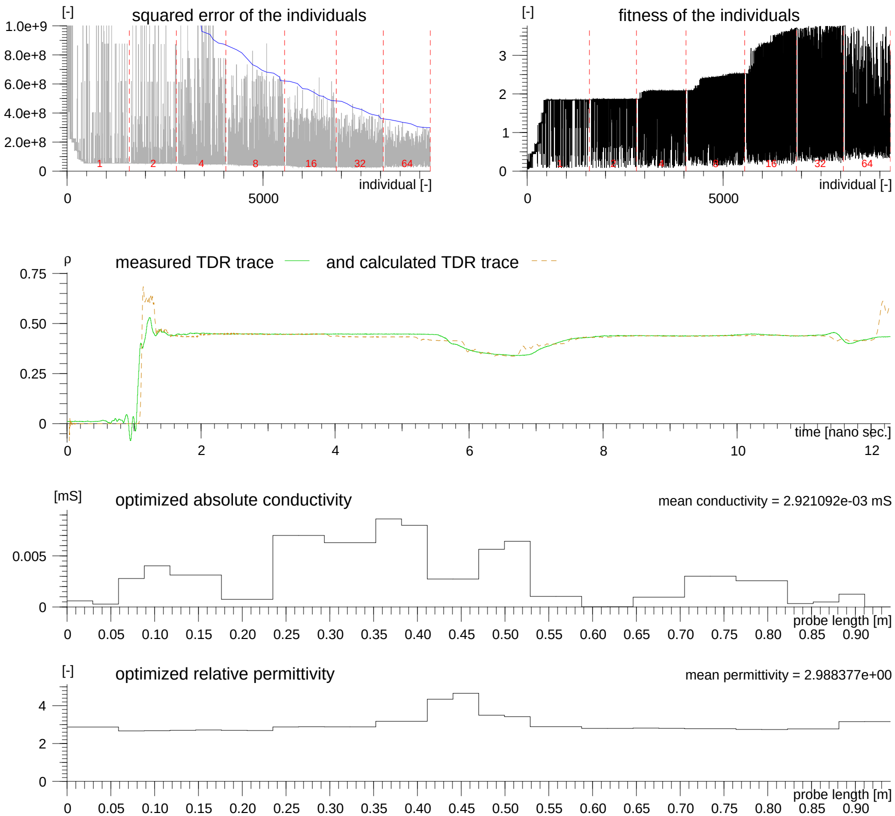

Fig. 15. Reconstruction of synthetic profile, $\theta_2 = 0.10$. Individual 7977 with error: $2.7 \cdot 10^7$ and fitness: 3.8.

HESSD

2, 1449–1502, 2005

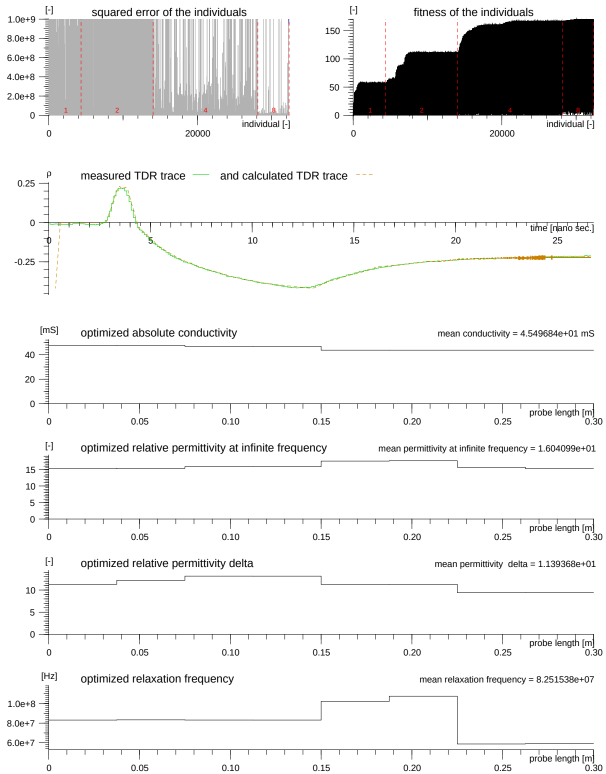

Fig. 16. Reconstructed TDR trace, measured at Grenzhof, Heidelberg, Germany in 1.41 m depth. Individual 32231 with error: $5.9 \cdot 10^5$, fitness: 171, terminal impedance: 600 Ω, and terminal capacitance $3.8 \cdot 10^{-17}$ F.

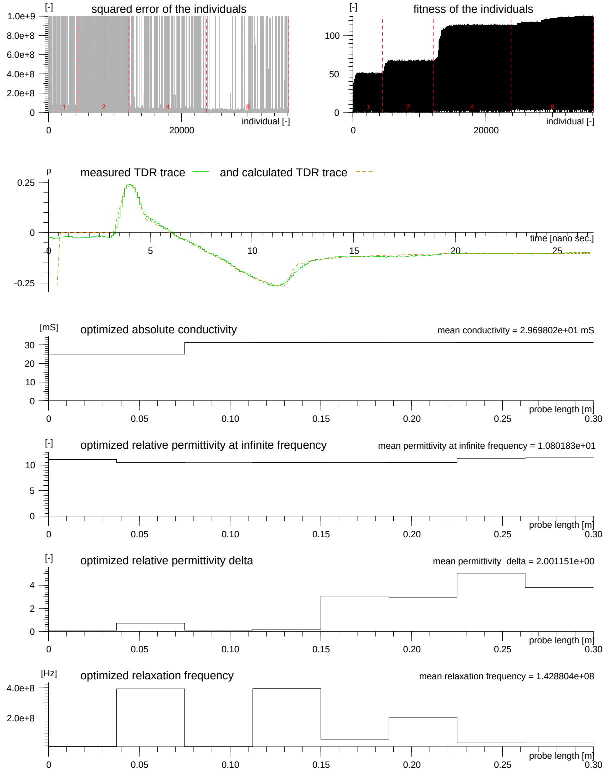

Fig. 17. Reconstructed TDR trace, measured at Grenzhof, Heidelberg, Germany in 0.72 m depth. Individual 35948 with error: $8.0 \cdot 10^5$, fitness: 125, terminal impedance: 189 Ω, and terminal capacitance $2.5 \cdot 10^{-17}$ F.

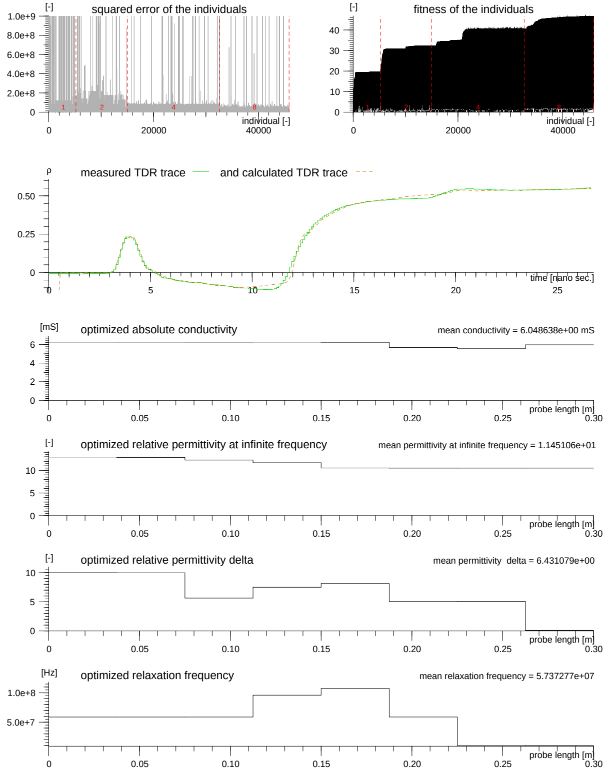

Fig. 18. Reconstructed TDR trace, measured at Grenzhof, Heidelberg, Germany in 0.13 m depth. Individual 45685 with error: $2.1 \cdot 10^6$, fitness: 47, terminal impedance: 580 Ω, and terminal capacitance $9.5 \cdot 10^{-18}$ F.

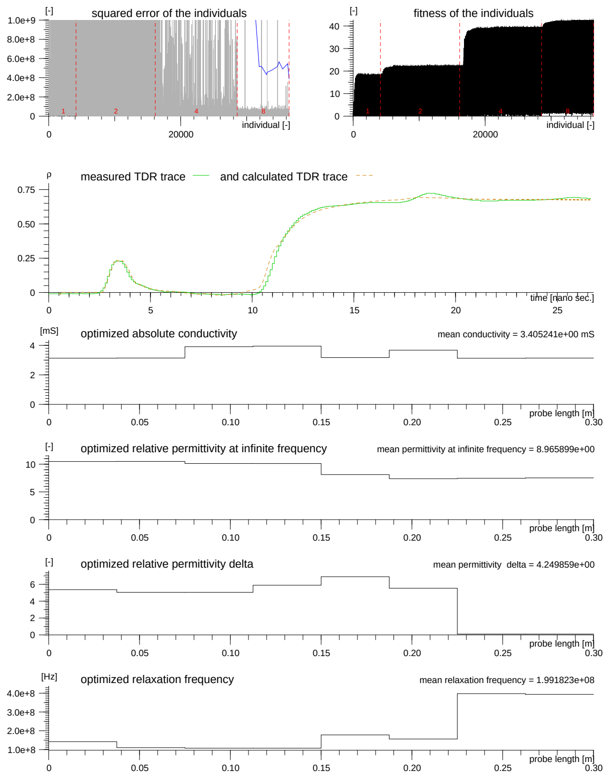

Fig. 19. Reconstructed TDR trace, measured at Grenzhof, Heidelberg, Germany in 0.30 m depth. Individual 36373 with error: $2.3 \cdot 10^6$, fitness: 43, terminal impedance: 600 Ω, and terminal capacitance $3.6 \cdot 10^{-17}$ F.